coatings

MDPI

Article

Chemical Vapor Transport Deposition of Molybdenum Disulfide Layers Using H_2O Vapor as the Transport Agent

Shichao Zhao *, Jiaxin Weng, Shengzhong Jin, Yanfei Lv and Zhenguo Ji *

College of Materials & Environmental Engineering, Hangzhou Dianzi University, Hangzhou 310018, China; weng_jiaxin@126.com (J.W.); wk_jsz@163.com (S.J.); lvyanfei@hdu.edu.cn

* Correspondence: zhaoshichao@hdu.edu.cn (S.Z.); jizg@hdu.edu.cn (Z.J.)

Received: 8 January 2018; Accepted: 14 February 2018; Published: 21 February 2018

Abstract: Molybdenum disulfide (MoS_2) layers show excellent optical and electrical properties and have many potential applications. However, the growth of high-quality MoS_2 layers is a major bottleneck in the development of MoS_2-based devices. In this paper, we report a chemical vapor transport deposition method to investigate the growth behavior of monolayer/multi-layer MoS_2 using water (H_2O) as the transport agent. It was shown that the introduction of H_2O vapor promoted the growth of MoS_2 by increasing the nucleation density and continuous monolayer growth. Moreover, the growth mechanism is discussed.

Keywords: chemical vapor transport deposition; molybdenum disulfide; monolayer; water; mechanism

1. Introduction

Molybdenum disulfide (MoS_2) layers, having unique optical and electrical properties, have attracted extensive interest in the fields of energy generation, electronics, and sensors [1–7]. The growth of large-scale, high-quality MoS_2 layers targeted for silicon integrated device fabrication is still challenging. Vapor deposition has been the predominant method for the growth of large-scale, continuous MoS_2 monolayer or few layers films in recent years [8–10]. Molybdenum oxides and sulfur are generally used as precursors of MoS_2. For example, Lee et al. heated MoO_3 powder in sulfur vapor and obtained MoS_2 monolayer and multi-layer films [11]. In this method, MoO_3 was first reduced by sulfur vapor to form MoO_{3-x}, which was then further reacted with sulfur vapor to form MoS_2 [12]. MoO_3 acted as a nucleation center promoting crystal growth as well as the introduction of crystal defects. The introduction of defects plays two important roles; one is to promote nucleation for multi-layer growth, and the other is to tailor the electrical properties [13–16]. The MoS_2 domains grown with this method showed different morphologies, e.g. triangle, hexagon, three-point star, as a function of the different atomic ratio of sulfur to molybdenum [17,18].

MoS_2 powder is another commonly used starting material. Wu et al. [19] heated MoS_2 powder at 900 °C in the center of a tube furnace and obtained a MoS_2 monolayer on an insulating substrate downstream of the precursor in a lower temperature zone (~650 °C). The usage of single-precursor MoS_2 powder as the source of Mo and S avoided the introduction of impurities and heterogeneous nucleation during the growth of MoS_2 flakes. Therefore, the MoS_2 monolayer showed a regular triangular shape and high optical quality. This vapor-solid growth method is suitable for the deposition of high-quality monolayer single crystal flake. However, in our recent work, we found that the nucleation is difficult to initiate and the growth temperature window is very narrow, ca. ~50 °C [20]. These issues could be attributed to the low vapor pressure of MoS_2 powder. The chemical vapor transport method was generally used for the growth of crystals with a solid precursor that has

low vapor pressure. For example, Pisoni et al. reported the growth of MoS_2 single crystals using I_2, Br_2, and $TeCl_4$ as transport agents [21]. The transport agent converts MoS_2 into high vapor pressure intermediates, which undergo the reverse reaction to deposit MoS_2 onto the substrate. However, the vapor transport agents used in this study are highly toxic and reactive, which could limit their widespread use.

To overcome this limitation, we have investigated ways to improve the nucleation density of MoS_2 using various additives. In this paper, we report the chemical vapor transport growth behavior of MoS_2 monolayer or multi-layer films by using MoS_2 powder as the precursor and water (H_2O) vapor as the transport agent. In the nucleation stage, H_2O vapor was introduced into the deposition system and acted as a chemical transport agent. Our mechanistic study suggests that water reacted with MoS_2 to form MoO_2, which promoted the nucleation of MoS_2. In the previously mentioned growth methods, the sulfur comes from the sublimation of sulfur or MoS_2 powder and the sulfur flow rate is out of control. Here, the sulfur was formed through the reaction of MoS_2 and water, which provides us a possible way to adjust the sulfur flow rate by controlling the water vapor flow rate. In the second stage, H_2O vapor was cut off and MoS_2 continuously grew through a simple physical vapor transport process. This novel approach combined the heterogeneous nucleation and homogeneous growth to control the crystal size and thickness of the MoS_2 layer. The thickness of the MoS_2 film obtained ranged from a monolayer to multiple layers. The lateral size of the single-crystal domain is up to 300 μm.

2. Materials and Methods

MoS_2 Layers Synthesis

MoS_2 was prepared by modifying a previously reported vapor deposition method using a silicon wafer with a 300-nm layer of oxide (SiO_2/Si) as the substrate [19]. The schematic of the vapor deposition setup is shown in Figure1. MoS_2 powder (99.5% purity, Aladdin, Shanghai, China) was used as the precursor. Before use, the precursor (0.5 g) was loaded into a small quartz glass boat (70 mm in length) and put in the center of the tube furnace (1 inch in diameter, Hefei Kejing Materials technology Co. LTD., Hefei, China). Before growth, the precursor was flushed under Ar/H_2 (70 sccm, H_2 5%, total pressure of 75 Torr. sccm: standard cubic centimeter per minute) for 10 min at room temperature to remove the air and water absorbed on the precursor. The substrate was put downstream close to the furnace wall.

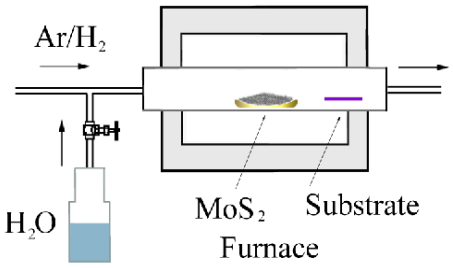

Figure 1. Schematic illustration of the MoS_2 growth setup.

For the MoS_2 growth, the precursor was heated to 1000 °C from room temperature in 30 min under Ar/H_2(75 Torr, Ar/H_2 70 sccm) and kept at 1000 °C for 1 h. The furnace was then turned off and cooled from 1000 °C to room temperature. During the above heating process, the temperature of the substrate ranged from 710 to 850 °C. The water (H_2O) vapor was introduced into the furnace by turning on/off the water valve, which connects the water tube and the Ar/H_2 inlet. For typical growth, the water valve was kept open during the whole heating stage. For studies on the influence of H_2O on the growth of MoS_2, we kept the valve open during the heating stage but limited the water exposure during the synthesis.

Optical microscope imaging of the sample was conducted with a Jiangnan MV3000 digital microscope (Nanjing Jiangnan Novel Optics Co. LTD., Nanjing, China). Tapping mode atomic force microscopy (AFM) was performed on an Agilent 5500 (Agilent Technologies, Palo Alto, CA, USA) in air. Raman spectrum and photoluminescence (PL) were acquired on a Renishawin Via micro-Raman spectroscope (Renishaw, London, UK) with a 532 nm solid-state laser at room temperature. X-ray diffraction (XRD) was carried on a Thermo ARLXTRA (Thermo Electron, Waltham, USA) and ultraviolet visible diffuse reflection spectroscopy (UV-Vis DRS, not including specular reflection) was performed on Shimadzu MPC-3100 (Shimadzu, Tokyo, Japan) with an integrating sphere.

3. Results and Discussion

3.1. MoS_2 Flakes Grown in the Presence of H_2O Vapor

MoS_2 flakes were prepared on the substrate using H_2O and MoS_2 powder as illustrated in Figure 2a. Figure 2b shows the separated triangular MoS_2 flakes grown on the SiO_2/Si substrate with the H_2O vapor valve kept open during the heating of the furnace and growth of the MoS_2 flakes. The thickness of the flakes ranged from monolayer to multiple layers. The triangles in dim and uniform color indicate the uniform monolayer MoS_2. The bright color triangles are attributed to multi-layer MoS_2 with a pyramid-shape structure. The flake lateral size ranged from ca. 20 to 40 μm.

The success of the growth and thickness of the MoS_2 flakes were confirmed by Raman spectroscopy. Figure 2c displays the typical Raman spectra of monolayer and multi-layer MoS_2 flakes corresponded to the images in Figure 2b. The E_{2g} and A_{1g} modes of MoS_2 were observed. The frequency difference between the E_{2g} and A_{1g} mode is thickness-dependent. With the increase of the layer number, the frequency difference valve will increase. The E_{2g} and A_{1g} peaks positions are at 385.0 cm^{-1} and 404.1 cm^{-1} (383.3 cm^{-1} and 409.1 cm^{-1}) with a frequency difference of 19.9 cm^{-1} (25.8 cm^{-1}), indicating that the thickness of flakes is monolayer (multi-layer) [22].

Besides Raman spectra, PL is generally used for the identification of the thickness of the MoS_2. Mak et al. studied the relationship between the PL quantum yield and layer number. They found that the PL quantum yield drops quickly with the increase of the layer number. Bulk MoS_2 is an indirect-gap semiconductor showing negligible PL. Few-layer MoS_2 shows weak PL due to the confinement effects. Monolayer MoS_2 is a direct-gap semiconductor giving out bright PL [23]. Figure 2d shows the typical photoluminescence spectra (PL) both of the monolayer and multi-layer MoS_2 flakes corresponded to the images in Figure 2b. The excitation wavelength was 532 nm. The PL peaks of monolayer MoS_2 are located at 674.5 nm and 622 nm, which are attributed to the A1 and B1 direct excitonic transition emission of the MoS_2 monolayer, respectively [9,17,24]. We observed that the PL intensity of the monolayer is much stronger than that of the multi-layer sample.

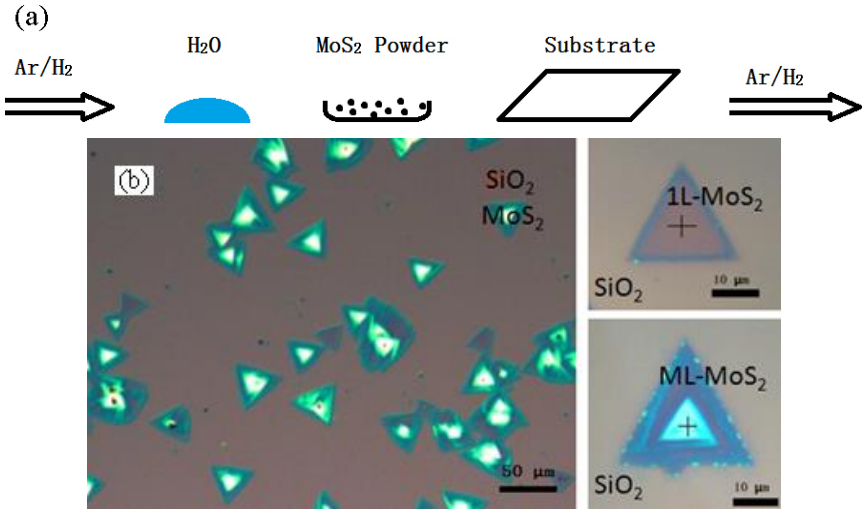

Figure 2. *Cont.*

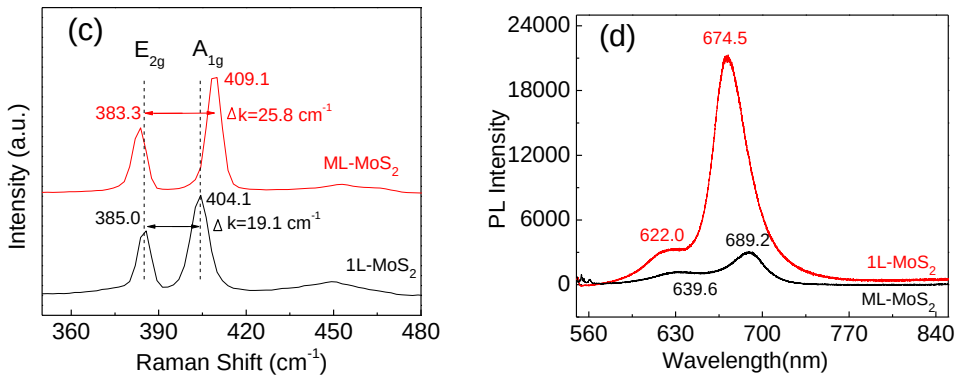

Figure 2. (**a**) Schematic illustration of the MoS_2 growth using H_2O and MoS_2 powder; (**b**) Optical images of MoS_2 grown on a SiO_2/Si substrate with H_2O vapor for 10 min; (**c**) Typical Raman spectra and (**d**) Photoluminescence (PL) spectra of the monolayer (1L-MoS_2) and multi-layer MoS_2 (ML-MoS_2) flakes according images shown in Figure 2b.

3.2. Effect of H_2O Vapor on the MoS_2 Layers Growth

To investigate the effect of H_2O vapor on the MoS_2 growth, we limited the time the synthesis was exposed to water vapor. After the precursors were heated to 1000 °C, the water valve was closed after a fixed amount of time during the growth stage: Figure 3a–d 0 min (least water exposure), Figure 3e–h 10 min, Figure 3i–l 20 min, and Figure 3m–p 60 min (most water exposure).

Shown in Figure 3a–d, the shape of the MoS_2 prepared without the introduction of H_2O is a separated island. Meanwhile in Figure 3e,i–k,m–o, continuous, large-area MoS_2 films were observed. This may be due to the presence of H_2O vapor, which enhanced the diffusibility of molybdenum and sulfur atoms at domain boundaries, resulting in the continuous growth of monolayer MoS_2. The large optical contrast in Figure 3e–p indicates the formation of multiple layers and/or clusters, which may be due to the formation of high heterogeneous nucleation density and the Stranski-Krastanov growth mode. The formation of heterogeneous nucleation will be discussed below. Besides the continuous film obtained as described above, the domain size of MoS_2 prepared with H_2O (shown in Figure 3f–h,p) was larger than those prepared without H_2O (shown in Figure 3b,c). Figure 4 shows the magnified optical image of the same sample that is shown in Figure 3e. The lateral size of the triangle-shaped MoS_2 flakes ranges from 24 μm to 372 μm. The average lateral size of the MoS_2 flakes prepared without H_2O introduction was 13 ± 6 μm, while the average size increased to 159 ± 80 μm based on the statistical calculation of the size of the isolated flakes shown in Figure 3a–h, respectively.

The water introduction also has an effect on the thickness of MoS_2 flakes. Based on the frequency difference (24.7 cm^{-1}, Figure S1) between the E_{2g} and A_{1g} mode of MoS_2 and uniform color contract, we can conclude that the MoS_2 flakes prepared without water exposure in Figure 3a–d is multi-layer. In contrast, in those samples prepared in the presence of water (Figure 3e–p), monolayer MoS_2 was observed (as discussed at the end of Section 3.2). Therefore, the introduction of water can reduce the thickness of the MoS_2 flakes.

It is reported that water molecules and carbon atoms can intercalate between the two-dimensional material and the substrate [25–27]. Although we do not have enough evidence to show the presence of the water intercalation in our sample at high growth temperature (710 °C to 850 °C), we suspect that the molecular structure of water vapor possibly intercalates into the interlayer of the MoS_2 flakes or the interface between the MoS_2 and SiO_2/Si substrate, which affects the absorption, desorption, and diffusion of the precursor atoms and even the final monolayer growth.

From Figure 3m–o, we can observe some bright features. The white spots are multi-layer MoS_2. The area with green and yellow color we suspected to be amorphous MoS_2, MoO_2, or even organic contamination. To reduce the organic contamination, the silicon wafer substrate was cleaned with hot piranha solution (7:3 concentrated H_2SO_4:35% H_2O_2) for 10 min at room temperature, and the vapor deposition system was flushed under Ar/H_2 to remove air-borne contamination before MoS_2 growth.

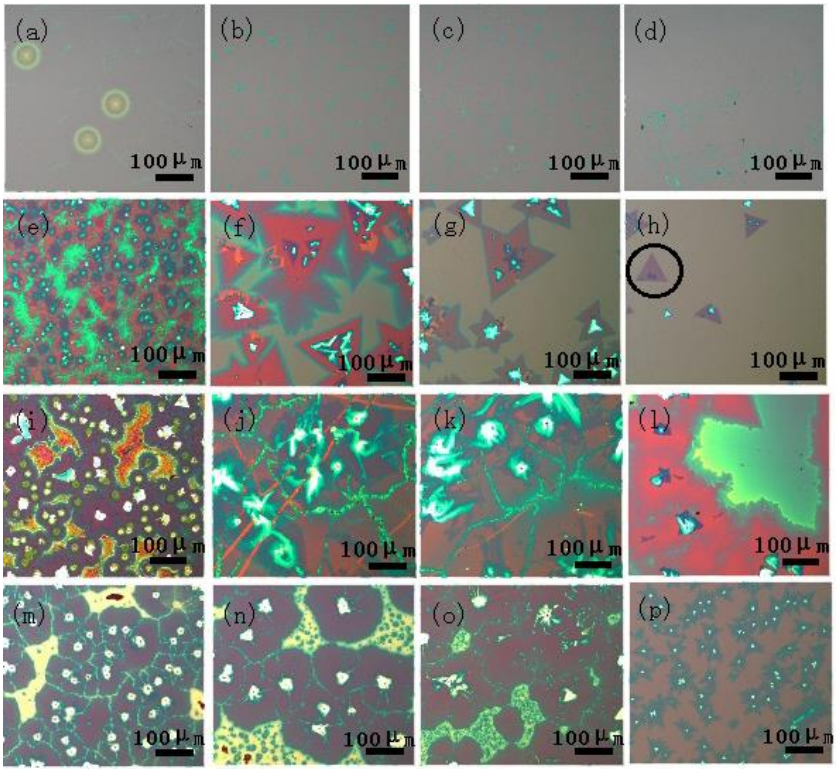

Figure 3. Optical images of the MoS_2 grown on a SiO_2/Si substrate with varying the amount of H_2O vapor released into the furnace. The images in each row are of the same sample but measured at different areas. From the left to right, the deposition temperature decreases as a result of the differences in the location. The amount of H_2O vapor into the furnace is controlled by adjusting the length of time that the H_2O valve is open: (**a**–**d**) 0 min, (**e**–**h**) 10 min, (**i**–**l**) 20 min, and (**m**–**p**) 60 min. For (**f**,**j**,**k**), we intentionally scratched the sample to show the contrast between the MoS_2 film and the SiO_2/Si substrate (bright orange color). The scale bars represent 100 μm.

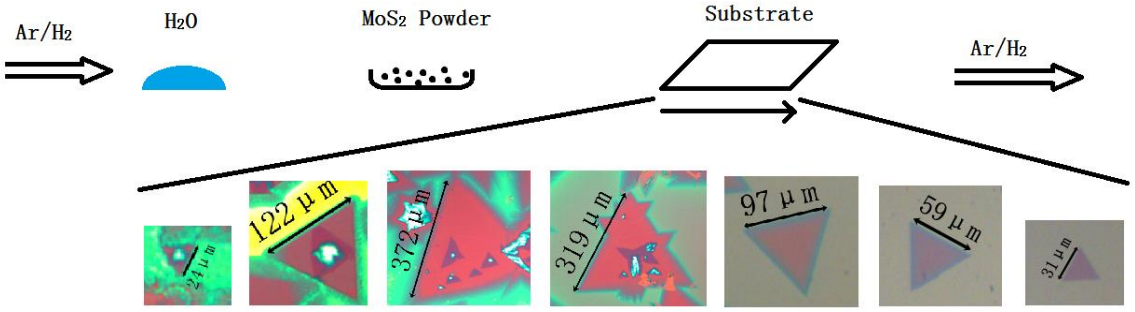

Figure 4. Magnified optical images of the same sample that is shown in Figure 3e. The images were measured at different locations. From left to right, the growth temperature was gradually decreasing.

Figure 5 shows the typical UV-Vis DRS of the MoS_2 film corresponding to the images shown in Figure 3e–h. The UV-Vis DRS peaks at 665 and 610 nm match the two PL emission peaks (Figure 2d), and are due to the characteristic A1 and B1 direct excitonic transitions of MoS_2, respectively [28].

AFM is a commonly used technique for two-dimensional material thickness measurement. Here, we conducted multiple scans of the thickness of the monolayer MoS_2 at an edge of the MoS_2 flake by AFM. Figure 6 shows the typical AFM image of the edge of the monolayer MoS_2 triangle shown circled in black in Figure 3h. A straight trench with a width of ca. 150 nm was observed on the substrate surface, which divided the substrate into two sections. The bottom of the trench is the SiO_2/Si substrate. The left side of the trench is MoS_2 particles, and the right side of the trench is monolayer MoS_2. The thickness of the MoS_2 flake is 0.9 ± 0.1nm (Figure 6, Figure S2, and Table S1), indicating that the flake is monolayer. This thickness value, although it significantly deviates from

the expected thickness of monolayer MoS_2 (0.615 nm), is consistent with other AFM measurements of single-layer MoS_2 deposited on a SiO_2 substrate [29,30]. In fact, the discrepancy that the measured value by AFM is larger than the theoretical value is common phenomena in the measurement of the thickness of two-dimensional monolayer materials, such as graphene [31]. The discrepancy was attributed to the instrument offset due to tip-substrate interaction as well as adsorbed molecules between the monolayer and the SiO_2 substrate [26,31]. From the AFM image in Figure 6, we can see that monolayer MoS_2 is smooth and continuous. We measured the root-mean-square (RMS) surface roughness over a 1 μm × 1 μm area. The RMS was 0.22 nm. The trench is probably formed through the rapid diffusion of MoS_2 nucleation along the direction perpendicular to the domain edge. Detailed study of the trench will be reported in future study. In addition to the trench, there are also many white particles on the surface of the MoS_2 flake. These particles should be MoS_2 formed during the growth of the MoS_2 flake, or even contaminations formed during the transport of the sample.

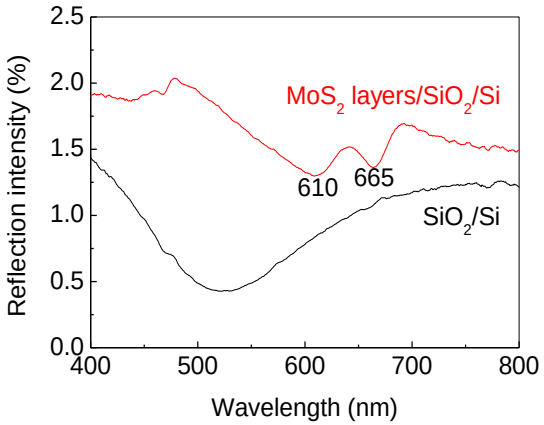

Figure 5. Typical ultraviolet visible diffuse reflection spectroscopy (UV-Vis DRS) of MoS_2 corresponding to the images in Figure 3b.

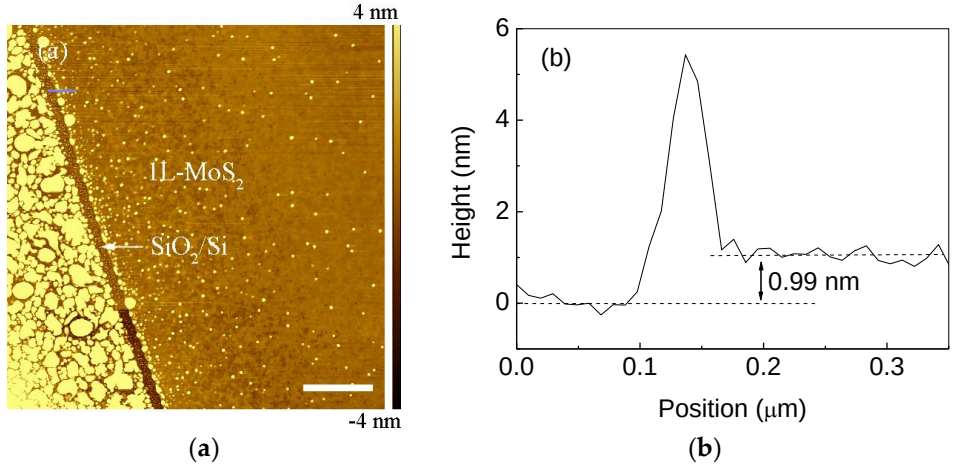

(**a**) (**b**)

Figure 6. Atomic force microscopy (AFM) image (**a**) and cross-section (**b**) (along the blue line marked in (a)) of monolayer MoS_2 grown on the SiO_2/Si substrate corresponding to the images in Figure 3h. The scale bars represent 1 μm in AFM image.

3.3. Mechanism of MoS_2 Growth in the Presence of H_2O Vapor

The results obtained in Figure 3 suggest that H_2O vapor promoted the growth of MoS_2 film. We hypothesized that the H_2O vapor reacted with MoS_2 powder to give molybdenum oxide. Then the molybdenum oxide evaporated and deposited on the substrate, acting as heterogeneous nucleation center, from which the molybdenum oxide reacted with sulfur at a lower temperature and transformed into the MoS_2 layer [12]. The following reactions should have occurred during the growth of MoS_2 [32]:

$$MoS_2 + 4H_2O \xrightarrow{1000\ ^\circ C} MoO_2 + H_2S + SO_2 + 3H_2 \quad (1)$$

$$2H_2S + SO_2 \xrightarrow{\Delta} 3S + 2H_2O \quad (2)$$

$$MoO_2 + 2S + 2H_2 \xrightarrow{\Delta} MoS_2 + 2H_2O \quad (3)$$

To verify this hypothesis experimentally, we used XRD to test the composition of the precursor annealed at 1000 °C for 20 h in H_2O vapor and H_2/Ar atmosphere. We indeed found that all of the XRD peaks in Figure 7 were indexed according to the monoclinic molybdenum dioxide (MoO_2) (JCPDS NO. 00-032-0671). This result agrees with our hypothesis that molybdenum oxide was formed. The growth process essentially is a chemical vapor transport process. The H_2O vapor acts as transport agent.

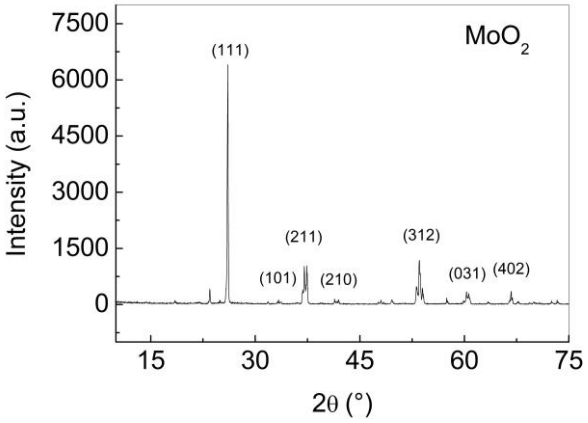

Figure 7. X-ray diffraction (XRD) of MoS_2 powder after annealing in Ar/H_2 and H_2O vapor at 1000 °C for 12 h. The peak positions are indexed to monoclinic MoO_2 (JCPDS NO. 00-032-0671).

4. Conclusions

In summary, we have successfully prepared monolayer/multi-layer MoS_2 through a H_2O vapor-modified vapor deposition method on a SiO_2/Si substrate. The growth of MoS_2 is highly sensitive to the presence of H_2O. The results reveal that H_2O increases the nucleation density of MoS_2 flakes. The Raman, PL, and AFM revealed that both monolayer and multi-layer MoS_2 were formed. Under extended water exposure, a continuous MoS_2 film was formed. Using XRD, we showed that MoO_2 was formed by the reaction between MoS_2 and water, which resulted in the observed enhancement in the nucleation and growth.

Supplementary Materials: The following are available online at http://www.mdpi.com/2079-6412/8/2/78/s1, Figure S1: Raman spectra of a multi-layers MoS_2 growth on the SiO_2/Si substrate tested at different locations, corresponding to the data in Figure 3a–d; Figure S2: AFM image of monolayer MoS_2 showing the edge of the domain. Scale bar represents 1 μm in AFM image; Table S1: Average height of the monolayer MoS_2 corresponding to the data in Figure S2 and Figure 6.

Acknowledgments: This work was supported by the Natural Science Foundation of Zhejiang Province, China Projects (LY16E020008) and Chinese NSF Projects (61106100). We thank Haitao Liu (Department of Chemistry, University of Pittsburgh, USA) for his kind assistance with data analysis and paper writing.

Author Contributions: Shichao Zhao conceived and designed the experiments and wrote the paper; Jiaxin Weng, Shengzhong Jin and Yanfei Lv performed the experiments; Shichao Zhao and Zhenguo Ji analyzed the data.

Conflicts of Interest: The authors declare no conflict of interest.

References

1. Buscema, M.; Barkelid, M.; Zwiller, V.; van der Zant, H.S.J.; Steele, G.A.; Castellanos-Gomez, A. Large and tunable photothermoelectric effect in single-layer MoS_2. *Nano Lett.* **2013**, *13*, 358–363.
2. Li, X.X.; Fan, Z.Q.; Liu, P.Z.; Chen, M.L.; Liu, X.; Jia, C.K.; Sun, D.M.; Jiang, X.W.; Han, Z.; Bouchiat, V.; et al. Gate-controlled reversible rectifying behaviour in tunnel contacted atomically-thin MoS_2 transistor. *Nat. Commun.* **2017**, *8*, 970.
3. Naylor, C.H.; Kybert, N.J.; Schneier, C.; Xi, J.; Romero, G.; Saven, J.G.; Liu, R.Y.; Johnson, A.T.C. Scalable production of molybdenum disulfide based biosensors. *ACS Nano* **2016**, *10*, 6173–6179.
4. Shavanova, K.; Bakakina, Y.; Burkova, I.; Shtepliuk, I.; Viter, R.; Ubelis, A.; Beni, V.; Starodub, N.; Yakimova, R.; Khranovskyy, V. Application of 2D non-graphene materials and 2D oxide nanostructures for biosensing technology. *Sensors* **2016**, *16*, 223.
5. Kalantar-zadeh, K.; Ou, J.Z. Biosensors based on two-dimensional MoS_2. *ACS Sens.* **2016**, *1*, 5–16.
6. Lopez-Sanchez, O.; Lembke, D.; Kayci, M.; Radenovic, A.; Kis, A. Ultrasensitive photodetectors based on monolayer MoS_2. *Nat. Nanotechnol.* **2013**, *8*, 497–501.
7. Tsai, M.L.; Su, S.H.; Chang, J.K.; Tsai, D.S.; Chen, C.H.; Wu, C.I.; Li, L.J.; Chen, L.J.; He, J.H. Monolayer MoS_2 heterojunction solar cells. *ACS Nano* **2014**, *8*, 8317–8322.
8. Robertson, J.; Liu, X.; Yue, C.L.; Escarra, M.; Wei, J. Wafer-scale synthesis of monolayer and few-layer MoS_2 via thermal vapor sulfurization. *2D Mater.* **2017**, *4*, 045007.
9. Kim, Y.; Bark, H.; Ryu, G.H.; Lee, Z.; Lee, C. Wafer-scale monolayer MoS_2 grown by chemical vapor deposition using a reaction of MoO_3 and H_2S. *J. Phys. Condens. Matter* **2016**, *28*, 184002.
10. Yu, Y.F.; Li, C.; Liu, Y.; Su, L.Q.; Zhang, Y.; Cao, L.Y. Controlled scalable synthesis of uniform, high-quality monolayer and few-layer MoS_2 films. *Sci. Rep.* **2013**, *3*, 1866.
11. Lee, Y.H.; Zhang, X.Q.; Zhang, W.J.; Chang, M.T.; Lin, C.T.; Chang, K.D.; Yu, Y.C.; Wang, J.T.W.; Chang, C.S.; Li, L.J.; et al. Synthesis of large-area MoS_2 atomic layers with chemical vapor deposition. *Adv. Mater.* **2012**, *24*, 2320–2325.
12. Liang, T.; Xie, S.; Huang, Z.T.; Fu, W.F.; Cai, Y.; Yang, X.; Chen, H.Z.; Ma, X.Y.; Iwai, H.; Fujita, D.; et al. Elucidation of zero-dimensional to two-dimensional growth transition in MoS_2 chemical vapor deposition synthesis. *Adv. Mater. Interfaces* **2017**, *4*, 1600687.
13. Bampoulis, P.; van Bremen, R.; Yao, Q.R.; Poelsema, B.; Zandvliet, H.J.W.; Sotthewes, K. Defect dominated charge transport and fermi level pinning in MoS_2/metal contacts. *ACS Appl. Mater. Interfaces* **2017**, *9*, 19278–19286.
14. McDonnell, S.; Addou, R.; Buie, C.; Wallace, R.M.; Hinkle, C.L. Defect-dominated doping and contact resistance in MoS_2. *ACS Nano* **2014**, *8*, 2880–2888.
15. Zhou, W.; Zou, X.L.; Najmaei, S.; Liu, Z.; Shi, Y.M.; Kong, J.; Lou, J.; Ajayan, P.M.; Yakobson, B.I.; Idrobo, J.C. Intrinsic structural defects in monolayer molybdenum disulfide. *Nano Lett.* **2013**, *13*, 2615–2622.
16. Addou, R.; Colombo, L.; Wallace, R.M. Surface defects on natural MoS_2. *ACS Appl. Mater. Interfaces* **2015**, *7*, 11921–11929.
17. Wang, S.S.; Rong, Y.M.; Fan, Y.; Pacios, M.; Bhaskaran, H.; He, K.; Warner, J.H. Shape evolution of monolayer MoS_2 crystals grown by chemical vapor deposition. *Chem. Mater.* **2014**, *26*, 6371–6379.
18. Yang, S.Y.; Shim, G.W.; Seo, S.B.; Choi, S.Y. Effective shape-controlled growth of monolayer MoS_2 flakes by powder-based chemical vapor deposition. *Nano Res.* **2017**, *10*, 255–262.
19. Wu, S.F.; Huang, C.M.; Aivazian, G.; Ross, J.S.; Cobden, D.H.; Xu, X.D. Vapor-solid growth of high optical quality MoS_2 monolayers with near-unity valley polarization. *ACS Nano* **2013**, *7*, 2768–2772.
20. Jin, S.Z.; Zhao, S.C.; Weng, J.X.; Lv, Y.F. Mn-promoted growth and photoluminescence of molybdenum disulphide monolayer. *Coatings* **2017**, *7*, 78.
21. Pisoni, A.; Jacimovic, J.; Barisic, O.S.; Walter, A.; Nafradi, B.; Bugnon, P.; Magrez, A.; Berger, H.; Revay, Z.; Forro, L. The role of transport agents in MoS_2 single crystals. *J. Phys. Chem. C* **2015**, *119*, 3918–3922.
22. Castellanos-Gomez, A.; Barkelid, M.; Goossens, A.M.; Calado, V.E.; van der Zant, H.S.J.; Steele, G.A. Laser-thinning of MoS_2: On demand generation of a single-layer semiconductor. *Nano Lett.* **2012**, *12*, 3187–3192.
23. Mak, K.F.; Lee, C.; Hone, J.; Shan, J.; Heinz, T.F. Atomically thin MoS_2: A new direct-gap semiconductor. *Phys. Rev. Lett.* **2010**, *105*, 136805.
24. Splendiani, A.; Sun, L.; Zhang, Y.B.; Li, T.S.; Kim, J.; Chim, C.Y.; Galli, G.; Wang, F. Emerging photoluminescence in monolayer MoS_2. *Nano Lett.* **2010**, *10*, 1271–1275.

25. Bampoulis, P.; Teernstra, V.J.; Lohse, D.; Zandvliet, H.J.W.; Poelsema, B. Hydrophobic ice confined between graphene and MoS_2. *J. Phys. Chem. C* **2016**, *120*, 27079–27084.
26. Varghese, J.O.; Agbo, P.; Sutherland, A.M.; Brar, V.W.; Rossman, G.R.; Gray, H.B.; Heath, J.R. The influence of water on the optical properties of single-layer molybdenum disulfide. *Adv. Mater.* **2015**, *27*, 2734–2740.
27. Kwiecinski, W.; Sotthewes, K.; Poelsema, B.; Zandvliet, H.J.W.; Bampoulis, P. Chemical vapor deposition growth of bilayer graphene in between molybdenum disulfide sheets. *J. Colloid Interface Sci.* **2017**, *505*, 776–782.
28. Sim, H.; Lee, J.; Park, B.; Kim, S.J.; Kang, S.; Ryu, W.; Jun, S.C. High-concentration dispersions of exfoliated MoS_2 sheets stabilized by freeze-dried silk fibroin powder. *Nano Res.* **2016**, *9*, 1709–1722.
29. Frindt, R.F. Single crystals of MoS_2 several molecular layers thick. *J. Appl. Phys.* **1966**, *37*, 1928–1929.
30. Li, H.; Zhang, Q.; Yap, C.C.R.; Tay, B.K.; Edwin, T.H.T.; Olivier, A.; Baillargeat, D. From bulk to monolayer MoS_2: Evolution of Raman scattering. *Adv. Funct. Mater.* **2012**, *22*, 1385–1390.
31. Zhao, S.C.; Surwade, S.P.; Li, Z.T.; Liu, H.T. Photochemical oxidation of CVD-grown single layer graphene. *Nanotechnology* **2012**, *23*, 355703.
32. Blanco, E.; Sohn, H.Y.; Han, G.; Hakobyan, K.Y. The kinetics of oxidation of molybdenite concentrate by water vapor. *Metall. Mater. Trans. B-Process Metall. Mater. Process. Sci.* **2007**, *38*, 689–693.